Research Article Vol. 28, No. 15 / 20 July 2020 / Optics Express 22036
Optics EXPRESS

Characterization of flat-fielding systems for quantitative microscopy

KHALID A. IBRAHIM, DORA MAHECIC, AND SULIANA MANLEY

Laboratory of Experimental Biophysics, École Polytechnique Fédérale de Lausanne, Route Cantonale, CH-1015 Lausanne, Switzerland

Abstract: Optical flat-fielding systems, such as field-mapping or integration-based beam shapers, are used to transform nonuniform illumination into uniform illumination. Thus, flat-fielding paves the way for imaging that is independent of position within a field of view and enables more quantitative analysis. Here, we characterize and compare three systems for homogenizing both widefield and multifocal illumination. Our analysis includes two refractive field-mapping beam shapers: PiShaper and TopShape, as well as one integration-based: Köhler integrator. The comparison is based on figures of merit including ISO-standard values, such as the plateau uniformity and edge steepness, transmission efficiency, stability of the beams along propagation and multifocal intensity, pitch, and point width. By characterizing and comparing existing beam shapers, we facilitate the choice of the appropriate flat-fielding solution and increase their accessibility for different applications.

1. Introduction

In widefield fluorescence microscopy, excitation light illuminates a sample labelled with fluorophores, and whose emission light is collected onto a camera. Commonly used illumination sources, such as lasers and light-emitting diodes (LEDs), have a spatially varying irradiance well-approximated by a Gaussian profile. This leads to a position-dependent excitation and emission of the sample, which causes the signal-to-noise ratio (SNR) of the resulting image to vary spatially. The SNR will also vary with time due to photobleaching, an effect which is also dependent on the local irradiance [1]. Furthermore, nonlinear effects such as photoactivation and photoswitching, used for single-molecule localization microscopy (SMLM) [2,3,4], have transition rates that depend on the local irradiance. All of these phenomena will lead to field-dependent image quality, which is problematic for quantitative analysis and interferes with increasing the field of view (FOV) through stitching together adjacent images.

Post-processing algorithms can correct for nonuniform illumination, however, they cannot compensate for variable SNR or nonuniformity in nonlinear effects such as photoswitching [5,6]. An intuitive way to render the illumination more uniform is to expand and crop the beam, keeping only the flatter central part of the beam. However, this approach wastes power, since it rejects, rather than homogenizes, the illumination. Another hardware-based approach termed "beam shaping" redistributes light to obtain a uniform beam profile, also known as a flat-top, through two major power-efficient strategies: field-mapping or beam integration. Field-mapping spatially reassigns light using either refractive or diffractive elements. Common refractive beam shapers use a pair of aspheric lenses arranged in either a Galilean or a Keplerian telescope configuration [7] and have been used in fluorescence microscopy to achieve higher uniformity imaging and to reduce artefacts [8,9,10]. Diffractive beam shapers use diffractive optical elements (DOEs) to transform the beam [11,12,13] with the same aim. In contrast, beam integration methods average out the nonuniform beam to obtain a flat-top. Examples of this technique include a shaking multi-mode fiber (MMF) [14,15] and the Köhler integrator, which uses a rotating diffuser and a pair of microlens arrays (MLAs) to create a parallel array of Köhler illumination channels that angularly split the input beam into subsections (beamlets) that are then superimposed by a

#395900 https://doi.org/10.1364/OE.395900
Journal © 2020 Received 23 Apr 2020; revised 5 Jun 2020; accepted 28 Jun 2020; published 10 Jul 2020

Optics EXPRESS

Fourier lens to produce a uniform intensity [16,17,18,19,20]. These approaches, among others, are summarized in Table 1.

Table 1. Overview and qualitative evaluation of hardware flat-fielding methods. €: <1k, €€: 1k-5k, €€€: >10k.

Flat-fielding method	Transmission efficiency	Multifocal applicability	Cost	Complexity	TIRF	Comment
Refractive field-mapping [8,9,10,22]	High	High	€€	Low	Yes	Commonly circular shape, stringent input beam requirements
Diffractive field-mapping [13]	Low	Low	€	Low	Not shown	Wavelength-sensitive
Köhler integrator [19,20]	Moderate	High	€€	Moderate	Not shown	Flexible input beam requirements
Shaking MMF [14,15]	Moderate	High	€€	Moderate	Yes	Coupling losses, motor functionality issues
ASTER [23]	High	Low	€€	High	Yes	Scanning-based
Waveguide-TIRF [24]	N/A	None	€	High	Only	Fabrication knowledge and laser coupling optics required
Borealis [25]	N/A	High	€€€	Low	Not shown	Proprietary
Spatial light modulation [26]	Low	Low	€€€	High	Not shown	Flexible flat-field shape

While these solutions come with intrinsic advantages and disadvantages (Table 1), their performance has not been directly compared. Furthermore, flat-fielding systems are commonly used for widefield illumination, but their applicability and performance for multifocal illumination have not been characterized. Here we characterize and compare three flat-fielding systems: the Köhler integrator and two commercial refractive beam shapers – PiShaper and TopShape, under both widefield and multifocal illumination conditions. These flat-fielding solutions offer several advantages (Table 1), including high uniformity, efficiency, and ease of use, as well as their applicability to multifocal illumination. MMFs could also be used for this purpose and operate in a similar fashion to the Köhler integrator, albeit lacking its design flexibility, and suffering from coupling losses and autofluorescence [21]. We expect that knowing the strengths and weaknesses of each of the three systems will allow non-expert users to identify the best suited solution for their experiment, enabling more users to take advantage of flat-fielding for quantitative imaging.

2. Results

2.1. Widefield illumination

We first evaluated the Köhler integrator, PiShaper and TopShape flat-fielding systems for their relative ease of use, which considers the number of elements, alignment and input beam requirements. PiShaper and TopShape consist of a single element (encompassing two aspheric lenses), which should be aligned to the optical axis, while the Köhler integrator is assembled from several elements (lenses, MLAs and a rotating diffuser), which should be co-aligned sequentially. Although aligning one element may appear simpler than multiple elements, refractive beam shapers are more sensitive to misalignment than typical optical elements such as lenses. This is because the field-mapping employed by refractive beam shapers requires a specific input beam – in this case, a Gaussian beam of a size specified by the manufacturer's design – to produce a high quality flat-top (Table 2). In contrast, we expect the Köhler integrator to be largely independent

Optics EXPRESS

of the input beam, since heterogeneities should be averaged out as long as sufficiently many microlens channels are used.

Table 2. Specifications of the flat-fielding systems.

Specification	Köhler integrator	PiShaper [27]	TopShape [28]
Collimated input/output	Yes/No	Yes/Yes	Yes/Yes
Input beam diameter ($1/e^2$), mm	Variable	5.9-6.0	10
Flat-field Size (FWHM), mm	Variable	6.0	14.6-14.8

How does the quality of the input beam affect the homogenization? Typically, the Köhler integrator produces a square output illumination (reflecting the shape of the MLA), while the PiShaper and TopShape produce round output illumination. We used a 647 nm laser (with $M^2 < 1.2$) of appropriate diameter as an input beam to each module and imaged their output profiles onto a CMOS chip camera (Methods). Using the unfiltered beam (Fig. 1(A)) produced low-uniformity profiles for PiShaper and TopShape, while the Köhler integrator was largely unaffected by the reduced input beam quality (Fig. 1(B)-(D), as reflected in their plateau uniformity and flatness factor values (Table 3). In this case, we do not report the edge steepness values because the PiShaper and TopShape beams were highly nonuniform, so the edge steepness value would vary with position. We then spatially filtered the input beam using a pinhole to produce a smooth Gaussian profile (Fig. 1(E)), which in turn improved the flat-top outputs, particularly for PiShaper and TopShape (Fig. 1(F)-(H), Table 3).

Table 3. Summary of results. Results in bold indicate the best quantitative performance, where applicable. NSF: non-spatially-filtered, SF: spatially-filtered, MF: multifocal.

Figure of merit	Köhler integrator	PiShaper	TopShape
Transmission efficiency	85.2%	**94.4%**	89.3%
Input beam deformation (Fig. 1)	Robust flat-fielding	Sensitive to shape and size	
Plateau uniformity (NSF, Fig. 1)	**0.0727**	0.2649	0.1815
Plateau uniformity (SF, Fig. 2)	**0.0621**	0.0899	0.0996
Flatness factor (NSF, Fig. 1)	**0.8442**	0.6053	0.5633
Flatness factor (SF, Fig. 2)	**0.8279**	0.7348	0.6725
Edge steepness (SF, Fig. 2)	0.2810	**0.2138**	0.3256
Stability with propagation (Fig. 3)	stable near focal plane	Flatness factor and quality decrease	
MF uniformity (Fig. 4)	**0.1294**	0.1653	0.2076
MF pitch deviation, µm (Fig. 4)	**0.09**	1.94	3.54
MF mean FWHM spot size, µm (Fig. 4)	36.1	21.90	**20.3**

Finally, we drastically degraded the input beam by cropping it in half (Fig. 1(I)) to imitate hard apertures within an optical path, and measured the output beam profiles. PiShaper and TopShape reproduced the deformations introduced in the input beam, generating cropped flat-top profiles with degraded uniformity (Fig. 1(J,K)). However, the cropping had a negligible effect on the uniformity of the flat-top produced by the Köhler integrator (Fig. 1(L)). These results are consistent with the different modus operandi implemented in these beam shapers. The refractive beam shapers have a one-to-one mapping from the input to the output, so when input sources are cropped, they will be missing in the output as well. Conversely, the Köhler integrator is based on field integration, a many-to-many mapping, such that when input sources are cropped, the output will integrate over fewer inputs to produce a flat-top profile of similar uniformity, albeit with a reduction in irradiance.

Optics EXPRESS

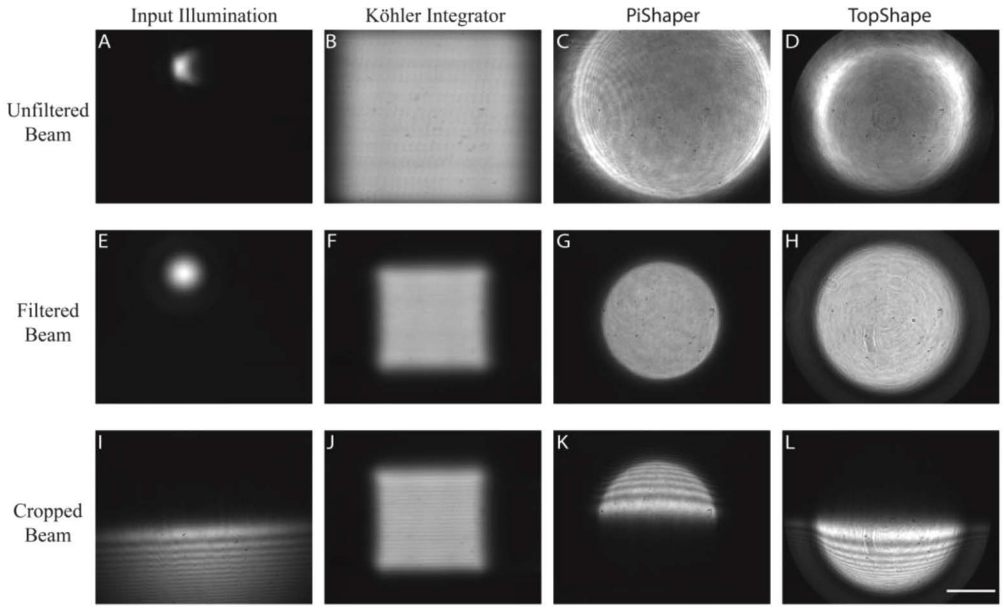

Fig. 1. Greyscale images of different conditions for the input illumination and the corresponding outputs produced by each of the three beam shapers. (A) Low quality input beam deviates from a Gaussian profile. (B-D) Flat-field outputs produced by the (B) Köhler integrator, (C) PiShaper and (D) Top shape, using a low quality input beam (A). (E) Spatial filtering produces a smoother Gaussian profile. (F-H) Flat-field outputs produced by the (F) Köhler integrator, (G) PiShaper and (H) TopShape, using the filtered Gaussian input beam (E). (I) The input beam is cropped in half. (J-L) Flat-field outputs for the (J) Köhler integrator, (K) PiShaper and (L) TopShape, using the cropped beam as input (I). Images (B,C) were taken before the introduction of a beam de-expander to the system. Scale bar, 1.5 mm.

To analyze the performance of the three beam shapers for widefield flat illumination, we used as figures of merit the edge steepness, plateau uniformity, and flatness factor, as defined in the ISO 13694:2000 standard [29]. The edge steepness signifies how sharply the intensity vanishes, while the plateau uniformity quantifies the extent of uniformity for a nearly flat-top profile. We also computed the flatness factor, which reflects heterogeneity in the intensity. These figures of merit are independent of flat-top beam size, intensity and shape.

To compare beam shapers, we considered the output produced by each using a spatially filtered input beam (Fig. 2(A-C)). We measured the intensity profiles along the horizontal and vertical midline, then extracted the 10% and 90% profile widths to compute the edge steepness as their difference normalized by the 10% width. The plateau uniformity was calculated by measuring the full-width at half-maximum (FWHM) of the image pixel intensity histogram (Fig. 2(E)) and normalizing by the maximum pixel intensity value. These standardized values range from 0 to 1, where 0 represents the ideal profile, and 1 the worst. The flatness factor was calculated as the ratio of the mean intensity value to the maximum value – such that a perfect flat-top profile would have a flatness factor of 1.

For edge steepness, we found that PiShaper had the best value (0.2138), followed by the Köhler integrator (0.2810) and TopShape (0.3256) (Table 3). The Köhler integrator achieved the best plateau uniformity and flatness factor (0.0621 uniformity, 0.8279 flatness factor), followed by PiShaper (0.0899 uniformity, 0.7348 flatness factor) and TopShape (0.0966 uniformity, 0.6725 flatness factor) (Table 3). These results support what one may conclude by visual inspection of

Optics EXPRESS

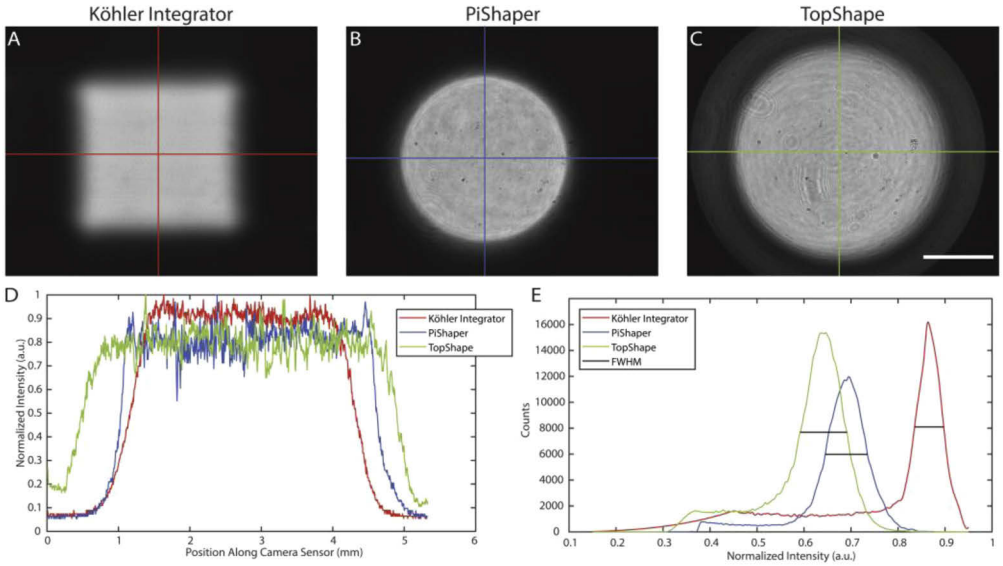

Fig. 2. Uniform greyscale images obtained from the three flat-topping systems under widefield illumination and their corresponding intensity profiles and histograms. (A) Köhler integrator. (B) PiShaper. (C) TopShape. The colored lines show the two locations where the intensity profiles are taken and then averaged. (D) Superimposed intensity profiles (here shown for the vertical line profile from A-C) of the three beam shapers. (E) Superimposed image (A-C) pixel grey-value histograms of the three beam shapers. The black bars represent the full-widths at half-maximum which are used to calculate the plateau uniformity. Scale bar, 1.5 mm.

the images, beam profiles and the histograms (Fig. 2). The images and beam profiles show that PiShaper has the sharpest edge, whereas the TopShape and Köhler integrator appear to roll-off more gradually.

We also measured the transmission efficiency (Table 3) of each beam shaper. PiShaper (94.4%) and TopShape (89.3%) had higher efficiency values than the Köhler integrator (85.2%), which is likely due to having fewer optical surfaces.

Another important aspect of creating flat-top illumination is ensuring it is maintained in the desired plane, usually the sample plane, displaced from the beam homogenizer. The PiShaper and TopShape produce collimated flat-top beams of a fixed size specified by the manufacturer (Table 2), whereas the Kohler integrator produces a flat-top illumination in a single plane, with a size that can be varied [17,18,30]. We studied the beam quality at varying distances for each system. In the case of the Köhler integrator, we measured the output beam at the focal plane of the Fourier lens where the flat-top beam is produced, as well as at positive and negative displacements from that plane (Fig. 3(A)). For this particular design, the focal plane was 10 cm from the output aperture, determined by the focal length of the Fourier lens. For PiShaper and TopShape, the measurements were done at increasing distances away from their output apertures (Fig. 3(B)).

To quantify the changes for each beam shaper, we measured the plateau uniformity, edge steepness and flatness factor as a function of distance. The Köhler integrator has a uniformity and flatness which are maintained even a few centimeters away from the focal plane. The edge steepness degrades more quickly at negative than positive displacements from the focal plane. For PiShaper and TopShape, the flat-top profile degrades as the distance increases, with the highest quality beam nearest to the output aperture. We noticed the emergence of concentric

Optics EXPRESS

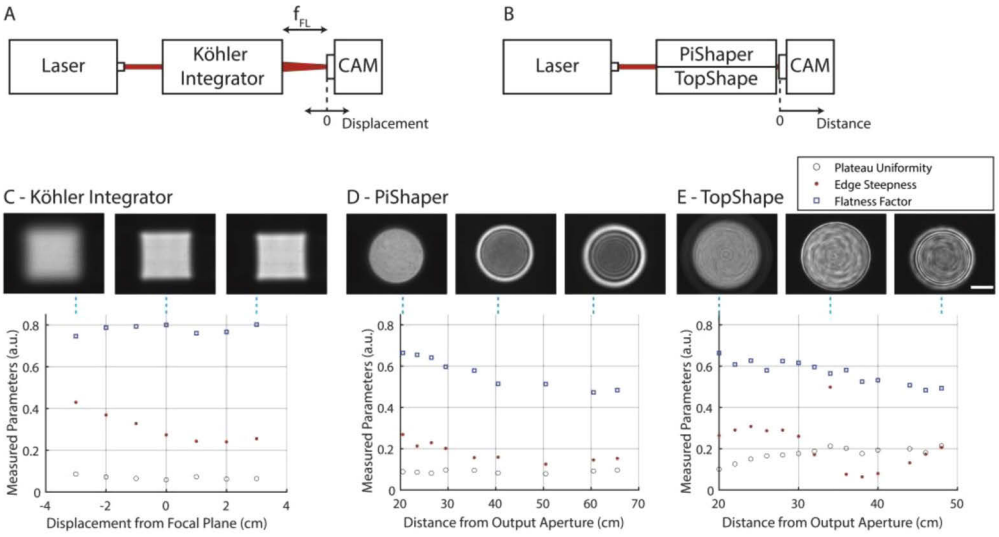

Fig. 3. Variation of the ISO standard values at varying propagation distance from the intended sample plane of each beam shaper. (A) Köhler integrator images are taken at positive and negative displacements from the focal plane where the flat-top is produced. (B) PiShaper and TopShape images are taken at increasing distances from their output apertures. (C-E) Plateau uniformity, edge steepness and flatness factor as a function of the displacement from the defined flat-field plane for the (C) Köhler integrator, (D) PiShaper and (E) TopShape. Scale bar, 1.5 mm.

rings for these refractive beam shapers, and a bright outer edge of increasing intensity. Thus, the edge steepness metric loses its relevance. Additionally, the plateau uniformity is negligibly affected by the small number of pixels in the higher-intensity edges. Therefore, it becomes more informative to consider the flatness factor, which is sensitive to higher intensity points, regardless of their location in the image or their density. PiShaper (Fig. 3(B)) and TopShape (Fig. 3(C)) both showed a trend of decreasing flatness, as expected.

2.2. *Multifocal illumination*

Techniques based on multifocal illumination emerged primarily as means of parallelizing point-scanning microscopy techniques – with optical sectioning and resolution increasing capabilities – to increase the throughput of scanning-based imaging. Examples of these techniques are spinning disk microscopy [31], multifocal structured illumination microscopy (MSIM) [32], and instant structured illumination microscopy (iSIM) [33]. When these techniques use a spatially nonuniform illumination source, the resulting multifocal excitation will follow a similar nonuniform envelope, leading to variations in the emission irradiance across the sample. Thus, the recorded image will have a spatially varying SNR, hindering quantitative analysis and producing artefacts and seams when stitching neighboring images. It is therefore important to correct for nonuniformities, not only in widefield, but also in multifocal illumination.

The output of each beam shaper was used to illuminate an MLA, generating multifocal excitation (Methods). We studied the spatial variations (Fig. 4) in the intensity (uniformity), spacing between each point and its neighbors (pitch) and spot size (Table 3). To assess the uniformity of the multifocal illumination, we computed the quartile coefficient of dispersion on the amplitudes of the multifocal points such that lower coefficients mean lower variation and therefore higher uniformity. The Köhler integrator, adapted for multifocal excitation by ensuring telecentricity and optimized spot size [20,30], had the best uniformity (0.1294), followed

Optics EXPRESS

by PiShaper (0.1653) and TopShape (0.2076), in agreement with the results for widefield illumination.

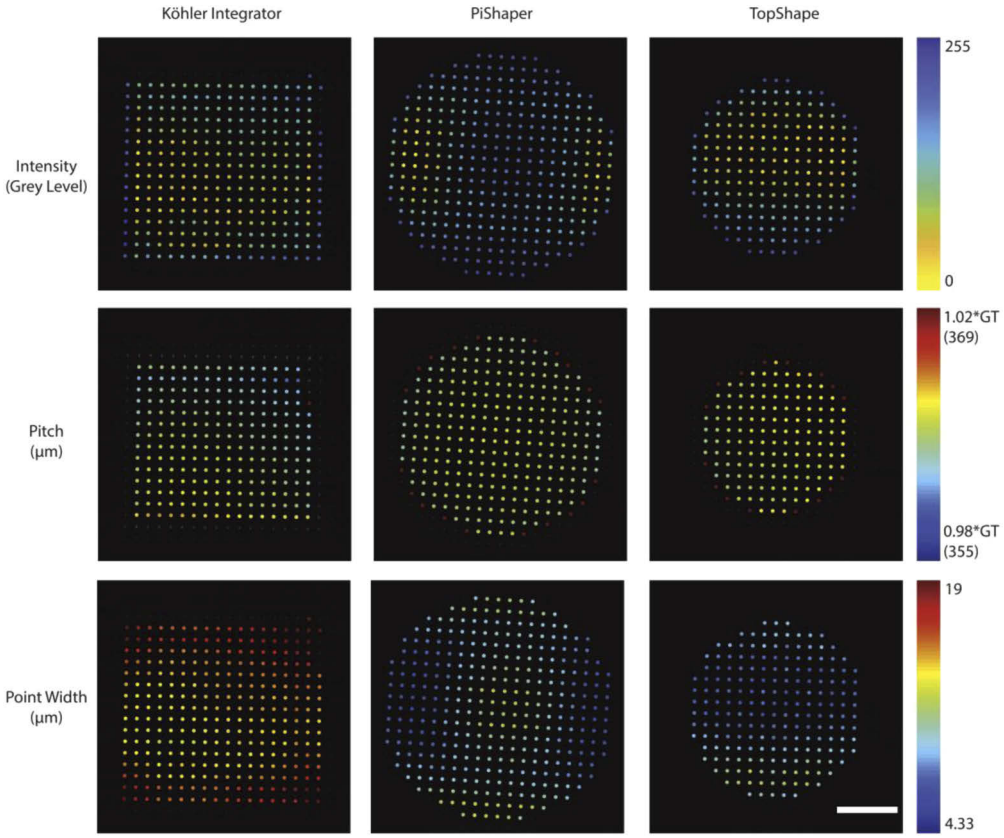

Fig. 4. Images of the multifocal illumination output of the three beam shapers, colored to represent quantitative variation. The three rows display the variation in intensity, pitch (spacing between points), and point width, respectively, with each column a different beam shaper. Scale bar, 1 mm.

Microscopes using multifocal excitation typically include other array components placed in conjugate planes, and all elements must be matched in pitch. Deviations in pitch introduce a cumulative error, which increases with distance away from the optical axis, gradually rejecting light and hence reducing homogeneity and transmission efficiency. To calculate the pitch, we measured the distance of each point to its orthogonal and diagonal neighbors, and compared them to the theoretical value set by the pitch of the MLA used to create the multifocal excitation. The Köhler integrator has the smallest difference between its mean pitch and the mean theoretical value (0.09 μm), followed by PiShaper (1.94 μm) and TopShape (3.54 μm).

The desired size of the multifocal spots will depend on the application, but too-large spots may compromise resolution. Thus, we compared the multifocal spot sizes for each flat-fielding system and compared them to a baseline with no beam shaping. We calculated the diffraction-limited spot size, w, of the input laser beam as $(4M^2\lambda f)/(\pi D)$, where M^2 is the beam quality factor, λ is the wavelength, f is the focal length of a microlens and D is the diameter of a microlens. This gives the $1/e^2$ spot diameter equal to 15.8 μm and equivalent to a FWHM of 9.3 μm. We also recorded an image of the multifocal pattern generated without any beam shaping elements, to measure experimentally the baseline spot size. The FWHM spot size from this image is

Optics EXPRESS

$w = 16$ µm. The measured FWHM spot sizes of the beam shapers are $w = 36.1$ µm (Köhler integrator), 21.9 µm (PiShaper) and 20.3 µm (TopShape). Both the theoretical and experimental diffraction-limited spot sizes are smaller than their flat-fielded counterparts.

Compared to the Köhler integrator, the refractive beam shapers' smaller spot sizes indicate a higher spatial coherence. This can be expected because the Köhler integrator's rotating diffuser used to scramble the incident coherent beam and average out interference patterns produces a partially coherent extended source, in contrast with PiShaper and TopShape. To estimate the spatial coherence of the beam shapers, we approximate the transverse coherence length, l_{coh} as $\lambda f/w$ for beams with limited spatial coherence [34]. Substituting the measured beam sizes into the equation yields coherence lengths of 53.6 µm (Köhler integrator), 88.3 µm (PiShaper) and 95.3 µm (TopShape). Nevertheless, contracting the beam diameter at the flat-fielding MLAs of the Köhler integrator has been used to control the resulting spot sizes [20], maintaining its utility for multi-focal microscopy.

3. Discussion

We characterized three flat-fielding systems, which transform Gaussian beams into flat-top beams: two commercial refractive field-mapping beam shapers – PiShaper and TopShape – and a Köhler integrator. For widefield illumination, the refractive beam shapers had 5-10% better transmission efficiency than the Köhler integrator, making them slightly more attractive for setups with weak light sources or applications requiring higher irradiance. However, the Köhler integrator had the best plateau uniformity and flatness factor, which are important properties for flat-top illumination. PiShaper had the best edge steepness, followed by the Köhler integrator and TopShape.

When flat-fielding systems are used to shape the input light of an imaging setup, the plateau uniformity and flatness factor reflect variations in the irradiance at the sample. Fluorescence microscopy is typically performed in a linear regime, where these variations will be replicated in the emission measured from the sample. For quantitative fluorescence microscopy applications – where collected emission intensities are used as readout of specific biological, chemical or physical properties – deviations from homogeneous illumination will introduce additional uncertainty to such measurements. Therefore, the reported plateau uniformities and flatness factors (Table 3), should be compared with other biological and measurement noise to determine whether they will be limiting. These differences could be a determining factor in some experiments, such as applications using emission irradiance for counting the numbers of proteins [35]. For nonlinear effects, such as the photoswitching processes in SMLM; higher variations in the sample irradiance could result in cycling between fluorescent and dark states on average across the FOV, but some fluorescent emitters not receiving the minimum irradiance locally. To maintain the single-molecule regime globally would require increasing the input power by the same amount as the variations. Therefore, the reported differences in the plateau uniformity represent the excess irradiance that would be necessary to ensure the necessary illumination conditions for SMLM. Finally, differences in edge steepness between flat-fielding solutions would affect the overlap that can be used between adjacent images that are stitched together to increase the FOV. Alternatively, when sharp edges are absolutely necessary, the lower-intensity edges would be cropped, so a difference in edge steepness would reflect the loss of power and size of the final beam.

We found that the flat-tops produced by PiShaper and TopShape were limited in stability with propagation distance, which could be problematic in cases where other optical elements prevent the sample from being placed near the output aperture – such as a tube lens and the objective. In contrast, the Köhler integrator maintains a satisfactory quality around the focal plane of the Fourier lens. The focal plane, where the flat-field is optimal, can be designed based on the overall setup to coincide with the sample plane by using the objective lens as the Fourier lens.

We studied the performance of these beam shapers for multifocal illumination, analyzing the variations in intensity, pitch and spot size for each. Having a uniform intensity minimizes the

Optics EXPRESS

appearance of artefacts in images, such as a checkerboard pattern due to variable intensities of the multifocal illumination. The Köhler integrator was once again the most uniform out of the three, and its pitch was closest to that of the MLA. A deviation of even a few micrometers is significant, as the cumulative error could lead to substantial separation from the desired pitch, such as the points being completely missed by a pinhole array further downstream in the microscope. We suspected that the refractive beam shapers might have a more erroneous pitch due to their propagation instability. PiShaper and TopShape had similar spot sizes. Both were smaller than the spots of the Köhler integrator, which might need to be masked to achieve better resolution, at the cost of reduced transmission efficiency. Nevertheless, we could generate usable multifocal excitation with each of the studied beam shapers, albeit with varying performance.

We analyzed the beam shapers on their own to characterize them without the effects of any external elements. They have already been used in microscopy setups [9,19,20,36], and we do not expect drastic changes in their performance when they are placed in that environment. It would be interesting to study the beam shapers' suitability for other modalities, such as total internal reflection fluorescence (TIRF) microscopy. The refractive beam shapers' smaller spot sizes verified their higher spatial coherence, which makes them more compatible for TIRF, where the light focused at the back focal plane (BFP) must be highly spatially coherent. There are other methods for flat-fielding that we have not characterized here, such as using diffractive beam shapers or multimode fibers. However, they either fall under the two families of flat-fielding systems that we characterized here: field-mapping and beam-integrations methods, or they are incompatible with multifocal illumination.

In addition to microscopy, flat-fielding is also important in holography to provide uniform illumination of spatial light modulators (SLMs) in computer-generated holography and to implement holographic data storage systems [37]. It is also widely used in the fields of photometry and radiometry [38]. A uniform illumination is crucial for creating well-controlled edges or patterns, in fields like photolithography, micromachining, laser ablation and welding [39,40,41,42,43,44]. The results of our analysis should help users make better-informed decisions on which beam shaper is most suited to a particular application. Furthermore, shedding light on the limitations of these flat-fielding systems, such as the instability of the refractive beam shapers along propagation or their deviating multifocal pitch, could stimulate solutions for these shortcomings or the development of new flat-fielding techniques that improve upon these systems.

4. Methods

4.1. Experimental setup

The laser source used (CUBE 640-100C, Coherent) has a wavelength of 647 nm, a maximum power of 100 mW and an M^2 value < 1.2. To magnify the laser beam size to the sizes required by PiShaper and TopShape, a 1.5x beam expander (f = 50 mm, f = 75 mm, Thorlabs), followed by a variable beam expander (2x – 5x, BE02-05-A, Thorlabs) are used. A pinhole (P50D, Thorlabs) is placed at the joint focal plane of the 1.5x beam expander lenses to spatially filter the beam. The Köhler integrator does not require a particular beam size, so the variable beam expander is not needed. Thus, one 6x beam expander (f = 50 mm, f = 300 mm, Thorlabs) is used (with a pinhole used for spatial filtering) so that the beam size is 6 mm, similar to the flat-top beam size produced by PiShaper.

The flat-topping systems which are characterized are PiShaper 6_6_VIS from AdlOptica, TopShape TSM25-10-D-B-6 from asphericon and a self-assembled Köhler integrator made of the following components: focusing lens (f = 80 mm, Thorlabs), rotating diffuser (2.5° ± 0.25° FWHM at 650 nm, 24-00066, Süss MicroOptics SA), collimating lens (f = 40 mm, Thorlabs), two flat-topping MLAs (300 µm pitch, 10mm x 10 mm, f = 4.78 mm, square lenses, 18-00157, Süss MicroOptics SA) and a Fourier lens (f = 300 mm, Thorlabs) [27,28]. PiShaper and TopShape were aligned using a 4-axis mount according to a method recommended by AdlOptica [45]. These

Optics EXPRESS

systems produce flat-top beams which are then imaged onto a camera (DCC1545M, Thorlabs) after being reduced by a factor of 0.6x by a beam de-expander (f = 50 mm, f = 30 mm, Thorlabs) to be of appropriate size for the sensor of the camera. An excitation MLA (300 µm pitch, 10mm x 10 mm, f = 8.72 mm, square lenses, 18-00221, Süss MicroOptics SA) is placed at the intended sample plane of each beam shaper to produce multifocal points when multi-point scanning illumination is being studied. A power meter is used to measure the input and output power of each system to calculate the transmission efficiency. The MLAs used in our experimental setup were chosen based on the design equations published in the literature [17,18].

4.2. Data analysis

MATLAB was used to process the images that were obtained using the beam shapers. The beams were segmented using thresholding to exclude the dark background to ease the processing. The pixel intensities are normalized to the maximum pixel intensity. To calculate the plateau uniformity, we plotted the grey-value histogram and spline-fitted the data then measured the FWHM of the peak. The flatness factor was computed as the mean of the thresholded intensities divided by the maximum value. We plotted the profiles at the midlines of the beam and computed the edge steepness for each case then took the average.

For the multifocal illumination images, we find the location of each focal point in the image and fit it to a 2D Gaussian to find the points' locations at subpixel precision and to calculate the spot sizes. To compute the pitch, we use an 8-nearest-neighbor search function, which finds the 4 orthogonal and 4 diagonal nearest neighbors. The mean values of the distance between each focal point to its nearest orthogonal and diagonal neighbors are calculated, respectively. We plot the variation in intensity, pitch and spot size with a value-based color map.

4.3. Alignment procedure

Standard alignment procedures were followed to align the mirrors and lenses in the system. A shearing interferometer was used to ensure proper collimation. PiShaper and TopShape were aligned using a procedure recommended by AdlOptica, the company making PiShaper, which ensures that such elements are aligned to the center of the beam, as well as angularly, meaning there is no tip or tilt relative to the beam [45]. This is accomplished by using a mount that can move independently in at least the 4 needed axes (to control horizontal and vertical movements, tip and tilt).

A tube with an input aperture of 2 mm and a variable-sized output aperture is put in place of each beam shaper. The beam is shined onto the camera in order to view the profile. Starting with a completely open output aperture, the mount screws are used to control the horizontal and vertical positions, while monitoring the beam profile to make sure the input beam is centered. Gradually, the output aperture is reduced (e.g. AdlOptica specify to go from 3 mm to 2 mm to 1 mm), and strictly angular adjustments are made, while monitoring the profile on the camera. Finally, the tube is removed and the beam shaper is placed instead. Some small potential alignments might be needed to get the optimum flat-top profile.

The procedure for aligning the Köhler integrator can be done in different ways. Here it is done first by aligning the Fourier lens to the optical axis, then aligning the two lenses that surround the rotating diffuser to the optical axis in a cage system configuration. The position of the second lens is marked; it is removed and the diffuser is inserted at the shared focal plane, then the lens is placed back. The diffuser's position can be moved later to find the position for an optimum flat-top profile. Next, the MLAs should be aligned; they are mounted in a cage-system and each MLA is mounted on a 2-axis kinematic mount which can control the transverse positions of the MLAs relative to the optical axis. The MLAs are placed roughly one lenslet focal length away from each other. The first MLA (closer to the input side) is adjusted transversally using the mount screws; proper alignment is obtained when slightly moving this MLA axially doesn't affect the

Optics EXPRESS

center or flatness of the profile. Rotational alignment of the two MLAs relative to one another should also be ensured; when the MLAs are properly aligned rotationally, a square-shaped beam should be observed.

Funding

European Research Council (819823, Piko); Schweizerischer Nationalfonds zur Förderung der Wissenschaftlichen Forschung (182429).

Acknowledgments

We thank all members of the LEB for helpful discussions and suggestions.

Conceptualization: all authors; data collection, analysis, visualization: KAI; validation, methodology: KAI, DM; supervision: DM, SM; writing: all authors.

Disclosures

The novel Köhler integrator for multi-focal excitation has been covered in a patent application filed by Ecole Polytechnique Federale de Lausanne (EPFL), with Dora Mahecic, Kyle Douglass and Suliana Manley as the inventors and is currently pending under patent application number PCT/EP2018/085228.

References

1. C. Eggeling, A. Volkmer, and C. A. M. Seidel, "Molecular photobleaching kinetics of Rhodamine 6G by one- and two-photon induced confocal fluorescence microscopy," ChemPhysChem **6**(5), 791–804 (2005).
2. M. J. Rust, M. Bates, and X. Zhuang, "Sub-diffraction-limit imaging by stochastic optical reconstruction microscopy (STORM)," Nat. Methods **3**(10), 793–796 (2006).
3. E. Betzig, G. H. Patterson, R. Sougrat, O. W. Lindwasser, S. Olenych, J. S. Bonifacino, M. W. Davidson, J. Lippincott-Schwartz, and H. F. Hess, "Imaging intracellular fluorescent proteins at nanometer resolution," Science **313**(5793), 1642–1645 (2006).
4. S. T. Hess, T. P. Girirajan, and M. D. Mason, "Ultra-high resolution imaging by fluorescence photoactivation localization microscopy," Biophys. J. **91**(11), 4258–4272 (2006).
5. J. A. Seibert, J. M. Boone, and K. K. Lindfors, "Flat-field correction technique for digital detectors," in *SPIE Proceedings Volume 3336, Medical Imaging 1998: Physics of Medical Imaging*, San Diego, 1998.
6. K. Smith, Y. Li, F. Piccinini, G. Csucs, C. Balazs, A. Bevilacqua, and P. Horvath, "CIDRE: an illumination-correction method for optical microscopy," Nat. Methods **12**(5), 404–406 (2015).
7. B. R. Frieden, "Lossless conversion of a plane laser wave to a plane wave of uniform irradiance," Appl. Opt. **4**(11), 1400–1403 (1965).
8. I. Khaw, B. Croop, J. Tang, A. Möhl, U. Fuchs, and K. Y. Han, "Flat-field illumination for quantitative fluorescence imaging," Opt. Express **26**(12), 15276–15288 (2018).
9. C. J. Rowlands, F. Ströhl, P. P. V. Ramirez, K. M. Scherer, and C. F. Kaminski, "Flat-field super-resolution localization microscopy with a low-cost refractive beam-shaping element," Sci. Rep. **8**(1), 5630 (2018).
10. F. Stehr, J. Stein, F. Schueder, P. Schwille, and R. Jungmann, "Flat-top TIRF illumination boosts DNA-PAINT imaging and quantification," Nat. Commun. **10**(1), 1268 (2019).
11. H. Kiriyama, M. Michiaki, Y. Nakai, T. Shimomura, H. Sasao, M. Tanaka, Y. Ochi, M. Tanoue, H. Okada, S. Kondo, S. Kanazawa, A. Sagisaka, I. Daito, D. Wakai, F. Sasao, M. Suzuki, H. Kotakai, K. Kondo, A. Sugiyama, S. Bulanov, P. R. Bolton, H. Daido, S. Kawanishi, J. L. Collier, C. Hernandez-Gomez, C. J. Hooker, K. Ertel, T. Kimura, and T. Tajima, "High-spatiotemporal-quality petawatt-class laser system," Appl. Opt. **49**(11), 2105–2115 (2010).
12. G. Račiukaitis, E. Stankevičius, P. Gečys, M. Gedvilas, C. Bischoff, E. Jäger, U. Umhoffer, and F. Völklein, "Laser processing by using diffractive optical laser beam shaping," J. Laser Micro/Nanoeng. **6**(1), 37–43 (2011).
13. L. Sacconi, E. Froner, R. Antolini, M. R. Taghizadeh, A. Choudhury, and F. S. Pavone, "Multiphoton multifocal microscopy exploiting a diffractive optical element," Opt. Lett. **28**(20), 1918–1920 (2003).
14. J. Deschamps, A. Rowald, and J. Ries, "Efficient homogeneous illumination and optical sectioning for quantitative single-molecule localization microscopy," Opt. Express **24**(24), 28080–28090 (2016).
15. Z. Zhao, B. Xin, L. Li, and Z.-L. Huang, "High-power homogeneous illumination for super-resolution localization microscopy with large field-of-view," Opt. Express **25**(12), 13382–13395 (2017).
16. R. Völkel, H. P. Herzig, P. Nussbaum, and R. Dändliker, "Microlens array imaging system for photolithography," Opt. Eng. **35**(11), 3323–3330 (1996).
17. M. Zimmermann, N. Lindlein, R. Voelkel, and K. J. Weible, "Microlens laser beam homogenizer: from theory to application," in *SPIE Proceedings Volume 6663*, Laser Beam Shaping VIII, San Diego, 2007.

Optics EXPRESS

18. R. Voelkel and K. J. Weible, "Laser beam homogenizing: limitations and constraints," in *SPIE Proceedings Volume 7102, Optical Fabrication, Testing, and Metrology III*, Glasgow, 2008.
19. K. M. Douglass, C. Sieben, A. Archetti, A. Lambert, and S. Manley, "Super-resolution imaging of multiple cells by optimized flat-field epi-illumination," Nat. Photonics **10**(11), 705–708 (2016).
20. D. Mahecic, D. Gambarotto, K. M. Douglass, D. Fortun, N. Banterle, M. L. Guennec, K. A. Ibrahim, P. Gönczy, V. Hamel, P. Guichard, and S. Manley, "Homogeneous multifocal excitation for high-throughput super-resolution imaging," *bioRxiv*, 2020.
21. J. A. Udovich, N. D. Kirkpatrick, A. Kano, A. Tanbakuchi, U. Utzinger, and A. F. Gmitro, "Spectral background and transmission characteristics of fiber optic imaging bundles," Appl. Opt. **47**(25), 4560–4568 (2008).
22. Coherent, "Efficient transformation of Gaussian beams into uniform, rectangular intensity distributions," [Online]. Available: https://www.coherent.com/assets/pdf/Efficient-Transformation-of-Gaussian-Beams-into-Uniform-Rectangular-Intensity-Distributions_FORMFIRST.pdf. [Accessed 1 June 2020].
23. A. Mau, K. Friedl, C. Leterrier, N. Bourg, and S. Lévêque-Fort, "Fast scanned widefield scheme provides tunable and uniform illumination for optimized SMLM on large fields of view," *bioRxiv*, 2020.
24. A. Archetti, E. Glushkov, C. Sieben, A. Stroganov, A. Radenovic, and S. Manley, "Waveguide-PAINT offers an open platform for large field-of-view super-resolution imaging," Nat. Commun. **10**(1), 1267 (2019).
25. Andor, "Enhanced illumination and imaging upgrade for CSU spinning disks," [Online]. Available: https://biochimie.umontreal.ca/wp-content/uploads/sites/37/2016/02/Borealis_Specifications.pdf. [Accessed 1 June 2020].
26. S.-Y. Chen, F. Bestvater, W. Schaufler, R. Heintzmann, and C. Cremer, "Patterned illumination single molecule localization microscopy (piSMLM): user defined blinking regions of interest," Opt. Express **26**(23), 30009–30020 (2018).
27. AdlOptica, "PiShaper 6_6 Manual," 2019.
28. asphericon, " https://www.asphericon.com/shop/en/beamtuning/a-topshape/tsm25-10-d-b-632.html," 2019. [Online].
29. ISO, "ISO 13694:2018, Optics and photonics — Lasers and laser-related equipment — Test methods for laser beam power (energy) density distribution," 2018.
30. P. Schreiber, S. Kudaev, P. Dannberg, and U. D. Zeitner, "Homogeneous LED-illumination using microlens arrays," in *SPIE Proceedings Volume 5942, Nonimaging Optics and Efficient Illumination Systems II*, San Diego, 2005.
31. R. Gräf, J. Rietdorf, and T. Zimmermann, "Live Cell Spinning Disk Microscopy," in *Microscopy Techniques* 95 (Springer, Berlin, Heidelberg, 2005) 57–75.
32. A. G. York, S. H. Parekh, D. D. Nogare, R. S. Fischer, K. Temprine, M. Mione, A. B. Chitnis, C. A. Combs, and H. Shroff, "Resolution doubling in live, multicellular organisms via multifocal structured illumination microscopy," Nat. Methods **9**(7), 749–754 (2012).
33. A. G. York, P. Chandris, D. D. Nogare, J. Head, P. Wawrzusin, R. S. Fischer, A. Chitnis, and H. Shroff, "Instant super-resolution imaging in live cells and embryos via analog image processing," Nat. Methods **10**(11), 1122–1126 (2013).
34. A. Schweinsberg, J. Kuper, and R. W. Boyd, "Loss of spatial coherence and limiting of focal plane intensity by small-scale laser-beam filamentation," Phys. Rev. A **84**(5), 053837 (2011).
35. J. S. Verdaasdonk, J. Lawrimore, and K. Bloom, "Determining absolute protein numbers by quantitative fluorescence microscopy," Methods Cell Biol. **123**, 347–365 (2014).
36. M. Hausmann, E. Wagner, J.-H. Lee, G. Schrock, W. Schaufler, M. Krufczik, F. Papenfuß, M. Port, F. Bestvater, and H. Scherthan, "Super-resolution localization microscopy of radiation-induced histone H2AX-phosphorylation in relation to H3K9-trimethylation in HeLa cells," Nanoscale **10**(9), 4320–4331 (2018).
37. A. Laskin, V. Laskin, and A. Ostrun, "Beam shaping for holographic techniques," in *SPIE Proceedings Volume 9200, Photonic Fiber and Crystal Devices: Advances in Materials and Innovations in Device Applications VIII*, San Diego, 2014.
38. P. Blattner and R. Voelkel, "Homogenous monochromatic irradiance fields generated by microlens array," in *10th International Conference on New Developments and Applications in Optical Radiometry (NEWRAD)*, Daejeon, 2008.
39. J. J. Toriz-Garcia, G. L. Williams, R. McWilliam, N. L. Seed, A. Purvis, F. B. Soulard, J. J. Cowling, and P. A. Ivey, "Vertical tracks on the sidewall of a silicon die using 3D holographic photolithography," J. Micromech. Microeng. **21**(8), 085034 (2011).
40. R. C. Y. Auyeung, H. Kim, N. A. Charipar, A. J. Birnbaum, S. A. Mathews, and A. Piqué, "Laser forward transfer based on a spatial light modulator," Appl. Phys. A **102**(1), 21–26 (2011).
41. B. Mills, J. A. Grant-Jacob, M. Feinaeugle, and R. W. Eason, "Single-pulse multiphoton polymerization of complex structures using a digital multimirror device," Opt. Express **21**(12), 14853–14858 (2013).
42. R. Voelkel, "Micro-optics: Key enabling technology for photolithography," in *2015 20th Microoptics Conference (MOC)*, Fukuoka, 2015.
43. D. J. Heath, T. H. Rana, R. A. Bapty, J. A. Grant-Jacob, Y. Xie, R. W. Eason, and B. Mills, "Ultrafast multi-layer subtractive patterning," Opt. Express **26**(9), 11928–11933 (2018).
44. R. Voelkel, U. Vogler, A. Bich, P. Pernet, K. J. Weible, M. Hornung, R. Zoberbier, E. Cullmann, L. Stuerzebecher, T. Harzendorf, and U. D. Zeitner, "Advanced mask aligner lithography: new illumination system," Opt. Express **18**(20), 20968–20978 (2010).
45. AdlOptica, Recommended alignment procedure for piShaper 6_6/Focal-piShaper 9.